Available online at www.sciencedirect.com
ScienceDirect
Thin Solid Films 516 (2008) 1913–1919
www.elsevier.com/locate/tsf

Cohesion and adhesion of nanoporous TiO_2 coatings on titanium wires for photovoltaic applications

J. Ramier [a], N. Da Costa [a], C.J.G. Plummer [a], Y. Leterrier [a], J.-A.E. Månson [a,*], R. Eckert [b], R. Gaudiana [b]

[a] *Laboratoire de Technologie des Composites et Polymères (LTC), Ecole Polytechnique Fédérale de Lausanne (EPFL), Station 12, CH-1015 Lausanne, Switzerland*
[b] *KONARKA Technologies AG, 116 John Street, Lowell, MA 01852 USA*

Received 21 September 2006; received in revised form 9 July 2007; accepted 13 August 2007
Available online 21 August 2007

Abstract

The working electrode of a dye-sensitized photovoltaic fiber is constituted of a porous TiO_2 coated titanium wire. The cohesion and adhesion of such a brittle oxide coating on the ductile metal substrate are identified as crucial factors in maintaining photovoltaic efficiency during textile manufacture and weaving operations. The influence of coating thickness on these factors has been investigated in the present work. The tensile mechanical characterization with *in situ* microscopic observations shows that two damaging processes are involved. For the smaller thickness, loss of adherence appears to be at the interface and inside the coating bulk. Cracks become visible in a random distribution in size and density and do not cross the entire coating circumference. Large patches of coating are still anchored on the wire. For the larger thickness no cohesive rupture in the coating bulk has been observed. The loss of adherence appears at the interface closed to the cracks and grows rapidly as the strain increases. Numerical investigations based on the finite element method permit to analyze the distribution and the combination of radial interfacial stress and circumferential coating stress and their influence on the observed damage.

Keywords: Titanium oxide (TiO_2); Titanium wire (Ti wire); Cohesion; Photovoltaic; Adhesion

1. Introduction

Titanium dioxide (TiO_2) thin films are employed in a wide range of application areas, including microelectronics, sensors, and catalysis and photovoltaic [1]. They are associated with a variety of deposition techniques and substrates, and a corresponding variety of film morphology. The most common processing routes are vapor deposition, plasma deposition, sol–gel processing, casting from aqueous solution [2] and spray pyrolysis deposition [3,4]. The substrates differ in both shape and composition, and include flat or cylindrical, rigid or flexible, brittle or ductile materials based on polymers, inorganic glasses or metals. In the present case, the focus is on the TiO_2 coated titanium wire that form the core of the working electrode in photovoltaic (PV) fibers based on dye-sensitized cell (DSC) technology [1,5]. The working electrode is embedded in an electrolyte together with a Ti counter electrode, and the resulting structure is coated with a transparent cladding to provide structural integrity and protection. The dye electrons are excited by solar energy and injected into the conduction band of TiO_2. They then move to the counter electrode *via* the external circuit, and regenerate the electrolyte by a redox reaction. Finally, the electrolyte regenerates the dye by a reduction reaction. Two PV fibers have been realized as explained by Ramier et al. [6] with two different TiO_2 coating thicknesses. The PV performance of the device with a 3 μm thick coating was 10 times lower than that obtained with a 10 μm thick coating. However the cohesive strength of the thicker coating is expected to be lower than that of the thinner one. In other words, a trade-off should be found in order to optimize the PV performance and the mechanical integrity of the device.

In fact, the DSC fibers are ultimately intended for the preparation of PV textiles. The manufacture of textiles generally

* Corresponding author. Tel.: +41 21 693 4281; fax: +41 21 693 5880.
E-mail address: jan-anders.manson@epfl.ch (J.-A.E. Månson).

0040-6090/$ - see front matter © 2007 Elsevier B.V. All rights reserved.
doi:10.1016/j.tsf.2007.08.057

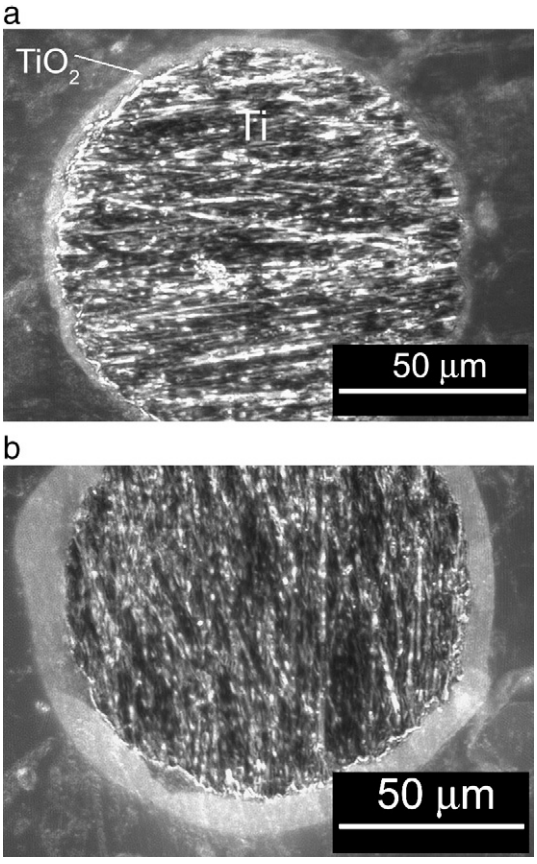

Fig. 1. Optical micrographs of cross-sections viewed in reflected light: (a) specimen No. 1, layer thickness, $t=3$ μm; (b) specimen No. 2, $t=10$ μm (reproduced from Ref. [6] with permission from Elsevier).

involves loading of the fibers in tension and in flexion, and internal stresses may also be induced during processing [6]. The mechanical resistance of the TiO_2 coating and its adhesion to the Ti substrate are therefore expected to play a key role in fiber performance. These properties are generally influenced by the roughness and cleanness of the substrate, the chemical affinity between the coating and the substrate, and the presence of cracks and other defects [7]. In the present case of a cylindrical geometry, a particularly important factor for the integrity of the interface between the Ti and the TiO_2 during deformation is expected to be the difference in Poisson's ratio (0.37 for Ti and 0.2 for monolithic TiO_2). The adhesion and fracture properties of coatings are often investigated using tensile tests [8–10], three [11] or four [12] point bend tests, peel tests [13] and scratch tests [11]. However, interpretation of such tests in terms of interfacial properties and the fracture response of the coating is difficult for a cylindrical geometry [14,15]. An alternative is to monitor damage *in situ* during deformation using, for example, scanning electron microscopy (SEM) [9] or optical microscopy [12,16,17]. The associated fragmentation behavior [18–21] may then be linked to the adhesion and fracture properties of the composite assembly.

The objective of this work has been to apply this approach to the working electrode of a DSC fiber [22] for different coating thicknesses, and to analyze the observations with the aid of finite element analysis (FEA) of the local stresses in the coating and substrate. The broad aim is to use the results to establish a link between the effects of mechanical solicitation and PV performance, and hence the conditions under which successful transformation of the fibers into textiles may be achieved.

2. Experimental methods

2.1. Materials

The two basic specimens used in this work were a 100 μm diameter Ti wire coated with a 3 μm (specimen No. 1) or a 10 μm (specimen No. 2) thick layer of nanoporous TiO_2 (Fig. 1), representing the working electrode of the complete DSC fiber assembly. The grade 1 titanium wire with Young's modulus of 100 GPa was supplied by Perryman Corporation and the TiO_2 layer was deposited using a proprietary technique [5]. The resulting TiO_2 particle agglomerates consisted mainly of anatase (tetragonal symmetry) and their average grain size was about 20 nm. The pore size was estimated by Saito et al. [23] to be between 15 and 25 nm and the porosity was 45 to 55%.

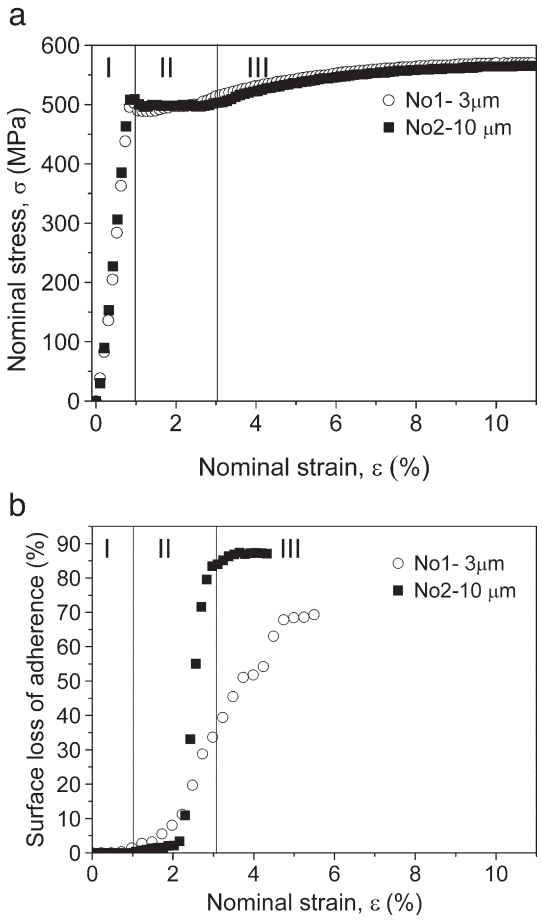

Fig. 2. Specimens No. 1 and No. 2 (Ti + TiO_2): (a) stress–strain curves; (b) damage represented in terms of loss in adhesion at the interface as a function of nominal strain.

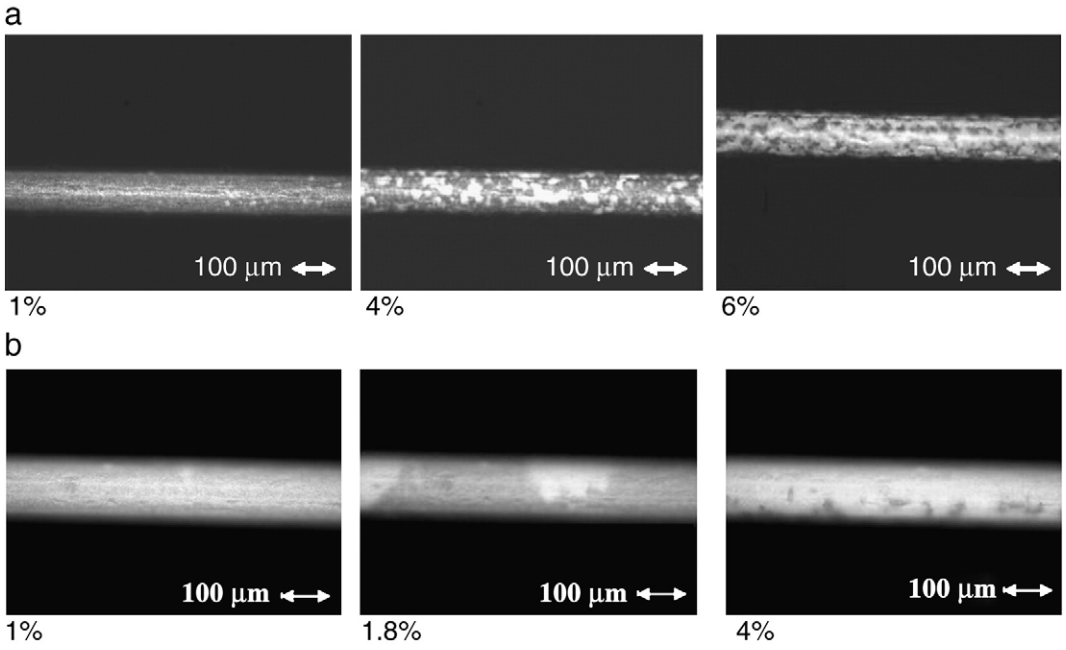

Fig. 3. Loss of adhesion between the TiO_2 layers and the Ti substrate: (a) specimen No. 1; (b) specimen No. 2 (reproduced from Ref. [6] with permission from Elsevier).

2.2. Mechanical testing and in situ microscopy

Preliminary tensile tests were carried out at room temperature at constant deformation rate (1 mm/min) using a tensile machine (UTS Testsysteme) equipped with a 100 N load cell and a linear variable differential transformer (LVDT) displacement sensor. Fragmentation tests were performed on 30 mm long wires at a constant deformation rate (1 mm/min) up to nominal strains of 10%, using a miniature tensile test apparatus (Minimat, Rheometric Systems) [20]. The apparatus was mounted on an optical microscope (Olympus BX-60) equipped for either bright or dark field observation in reflected light, and images of the specimen were recorded at an acquisition rate of 1 Hz. This permitted detailed monitoring of crack formation in the coating and loss of adhesion. Further analysis was carried out using SEM (XL-30 FEG, Philips) operated at 10 kV. *In situ* observations were made using a small tensile machine equipped with an LVDT displacement sensor and a force cell. To observe the fragmentation process during bending, the wires were wound onto circular bars with different diameters. Thus the minimum radius of curvature at which the cohesion and adhesion of the coating were maintained could be determined. FEA simulations were carried out using the Comsol software package in order to determine the effective interfacial stresses in the wires during deformation.

3. Mechanical and morphological characterization during tensile loading

Typical results from tensile tests on specimens No. 1 and No. 2 are shown in Fig. 2a along with the corresponding *in situ* damage analysis in Fig. 2b. The stress–strain curve may be divided into different regimes. The first regime (I) (between 0% and approximately 1% strain) involved quasi-linear deformation and corresponded to the elastic deformation of the titanium electrode (Ti). A few micron-sized cracks appeared in the TiO_2 coating at about 0.5% strain as shown in Fig. 4a. A regime of nearly constant

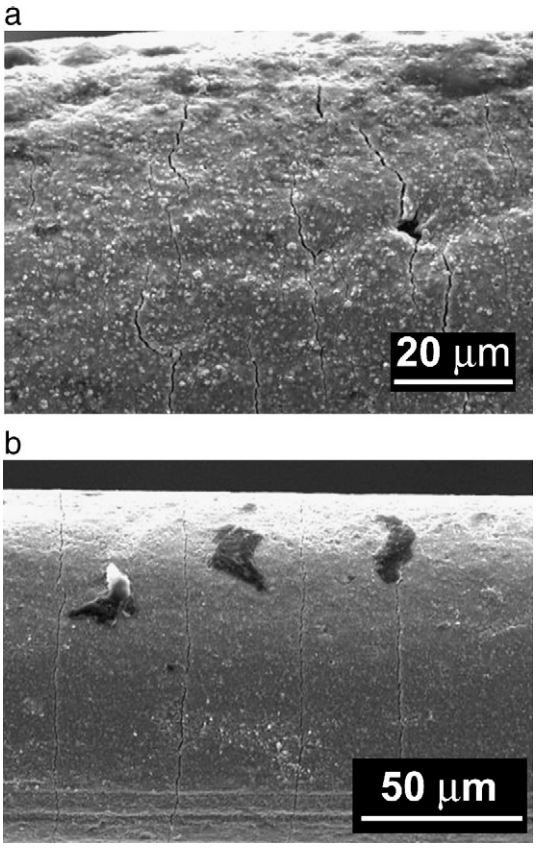

Fig. 4. SEM of cracks in the TiO_2 layers; (a) specimen No. 1 (1% strain); (b) specimen No. 2 (0.5% strain; reproduced from Ref. [6] with permission from Elsevier).

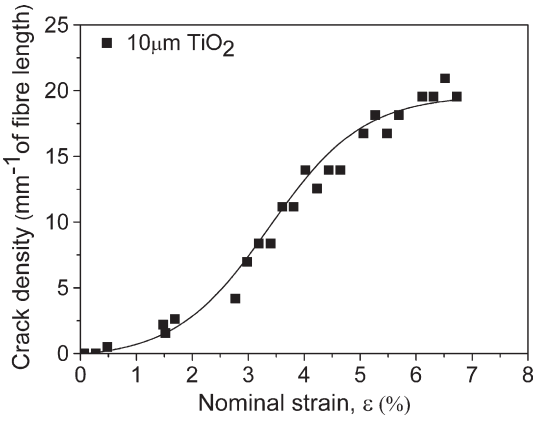

Fig. 5. Crack density in the TiO_2 coating of specimen No. 2 as a function of nominal strain.

stress (II) was then observed from 1% up to approximately 3% strain, which corresponded to the onset of the plastic deformation in the Ti. As shown in Fig. 2b, this regime was associated with damage in the form of loss of adhesion between the wire and the TiO_2 coating, as well as cohesive failure of the coating itself. Two different mechanisms of loss in adhesion were observed for the two different thicknesses of TiO_2. For specimen No. 1 (thickness 3 μm), loss in adhesion initiated in white patches (Fig. 3), apparently propagating from defects such as local agglomerations of the TiO_2. For specimen No. 2 (thickness 10 μm), on the other hand, loss in adhesion initiated around microcracks, which were only visible by SEM (Fig. 4b), and then propagated into rest of the specimen (at between 1% and 3% deformation). The overall loss of adhesion in terms of the fiber surface area was lower for the smaller TiO_2 thickness, *i.e.* 70% and 85% for specimens Nos. 1 and 2, respectively.

Cracks appeared for both coating thicknesses, but the crack morphologies were different in each case. As shown in Fig. 4a, the cracks were relatively short in specimen No. 1, and did not extend around the whole of specimen circumference. In specimen No. 2, the cracks appeared irregularly along the fiber, with relatively high concentrations in some areas, but the crack density (CD) became more uniform as the strain increased. The individual cracks extended around the whole circumference of the wire (Fig. 4b). At this stage, the cracks were spaced periodically so that the resulting fragments of coating were all close to 50 μm in length (as measured along the fiber axis). In Fig. 5, the crack density for specimen No. 2 is shown as a function of strain, counting only circumferential cracks. At deformations beyond 3%, where the stress increased slightly, the cracks continued to widen at a density close to 20 per mm of fiber (Figs. 4b and 5). In the final stages of the deformation process, the fragmentation morphologies of the coatings in specimen Nos. 1 and No. 2 were also different, reflecting the differences in crack morphology described above. As shown in Fig. 6a, in specimen No. 1, large fragments of the coating remained attached to the Ti substrate, whereas in specimen No. 2, the coating underwent extensive failure at the interface, with only residual anchoring between the Ti and the TiO_2.

4. Analysis

4.1. Cohesive properties

The tensile strength of the coating, σ_{max}, which, in case of brittle ceramic materials, depends on the behavior of microcracks under stress, was assumed to follow the Weibull weakest-link model with a single population of defects (*e.g.*, volume defects) [24]:

$$\sigma_{max}(l) = \sigma_0 (l/l_0)^{-1/m} \Gamma(1 + 1/m). \quad (1)$$

Where l represents the length of a coating fragment, l_0 is a normalization factor (chosen equal to 1 μm), Γ is the gamma function, σ_0 is the Weibull scale factor and m is the Weibull shape factor (or Weibull modulus). The Weibull parameters were determined from the data 1/CD *vs* coating stress, plotted in logarithmic coordinates [20]. Note that, in case residual stress are present, the value of σ_{max} derived from Eq. (1) represents an apparent strength, and is in fact a combination of an intrinsic strength and of internal stresses [25].

The Weibull modulus and scale factor were found to be equal to 1.2 and 490 MPa, respectively. The value of the modulus is very low, compared to that of ceramic materials, usually found to be in the range from 5 to 20. The Weibull modulus of porous TiO_2 coatings was reported to be larger than 5 [26], although it

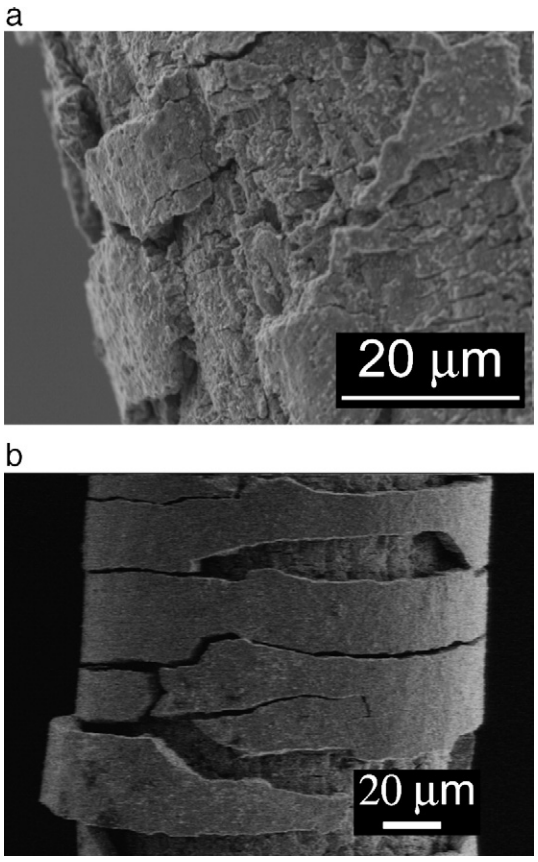

Fig. 6. SEM of damage and loss in adhesion of the TiO_2 film at 5% strain: (a) specimen No. 1; (b) specimen No. 2 (reproduced from Ref. [6] with permission from Elsevier).

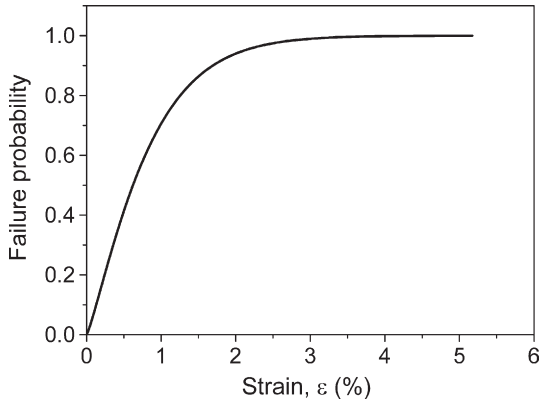

Fig. 7. Cumulative failure probability of specimen No. 2 (10 μm thick nanoporous TiO_2 coating) under tensile strain.

should be noticed that the values were determined from microhardness tests. The failure probability of the present coating under tensile strain depicted in Fig. 7 reflects the broad distribution of defects and related strength of the nanoporous structure. Due to the early occurrence of interfacial failure, the cohesive strength of the TiO_2 coating at critical length of the stress transfer process (*i.e.*, at fragmentation saturation [20]) could not be determined. Instead, a lower bound estimate was derived using (Eq. (1)) taking as the critical stress transfer length, the inverse of the maximum measurable crack density (20 mm^{-1}, Fig. 5), and found to be close to 4 GPa. This estimation is in the high range for porous ceramic materials. Thus, a reduction of large flaws through process optimization should considerably improve the cohesive properties of the nanocomposite coating. It is interesting to point out that, in spite of this low tensile strength, the performance of PV fiber devices only marginally degraded due to cracking of the TiO_2. Rather, it was the failure of the TiO_2/Ti interface that controlled the loss of PV performance, to which we now turn our attention.

4.2. Adhesive properties

It was demonstrated in a recent work [6] that the loss of adherence between the TiO_2 coating and the Ti wire was the main factor, which controlled the loss of PV performance of the fiber. The results of Section 3 indicate that for the lower TiO_2 layer thickness (3 μm), subsequent to the onset of cracking in the coating, delamination-type failure occurred both at the interface and in the bulk of the coating, with partial fragment spallation. Thus large patches of coating (up to 10 μm in diameter) remain attached to the Ti wire even at large deformations. For the higher coating thickness (10 μm), on the other hand, cohesive rupture was not observed in the bulk of the coating. In this case, loss of adhesion appeared at the interface adjacent to the cracks and propagated rapidly as the strain increased. These differences in damage morphology may be understood in terms of changes in the distribution of the interfacial radial stress, σ_R, and of the circumferential coating stress, σ_θ, as sketched in Fig. 8 (Shiao and Shieu [27]). The difference in Poisson's ratio between the Ti core (0.37) and the TiO_2 coating (0.2 for monolithic TiO_2) implies that tensile radial

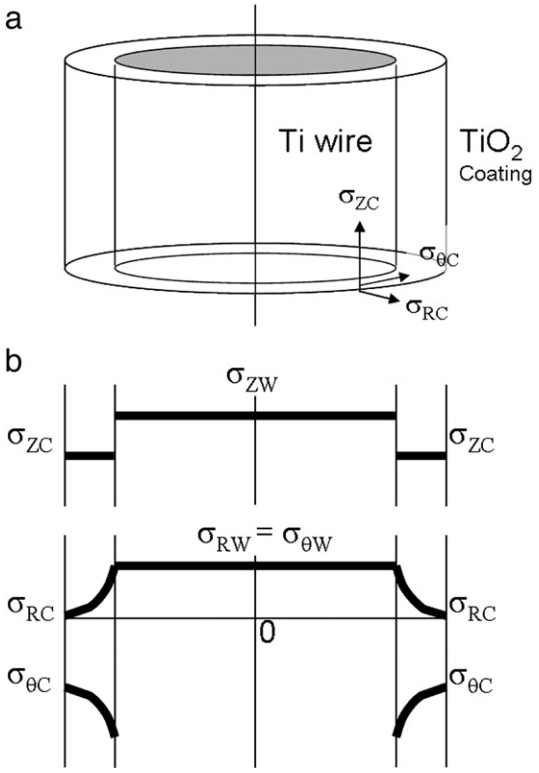

Fig. 8. Schematic representation of (a) the fiber (TiO_2 coated Ti wire) and (b) the stress distribution expressed in polar coordinates.

stresses should develop at the interface during tensile deformation, which are expected to contribute to the loss in adhesion (Fig. 8b). These stresses will in general depend strongly on the layer thickness.

FEA was used for the calculation of the stresses between the TiO_2 and the Ti during tensile testing and bending. The analysis was restricted to the elastic regime (strains below that at which the Ti undergoes plastic deformation), and the integrity of the coating was maintained during tensile deformation in z direction (the tensile stress σ_Z will fall to zero when circumferential cracks appear). As a first step, it was necessary to estimate the modulus of the porous TiO_2 coating, which was inferred from the known Young's modulus of the Ti wire and the TiO_2 coated Ti wire. The value obtained for the TiO_2 coating was 58 GPa, which is very

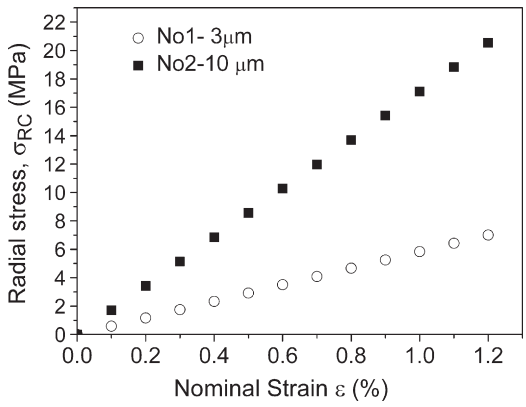

Fig. 9. FEA simulation of the radial stress at the interface.

much lower than the value for bulk TiO_2 (230 GPa), a result of the high porosity of the TiO_2 coating.

Fig. 9 shows the calculated σ_R as a function of tensile strain, based on the above values for Young's moduli and Poisson's ratios, indicating a linear dependence in the regime shown. In specimen No. 1 (3 μm), σ_R was about one third of the value calculated for specimen No. 2 (10 μm). In this latter case, at 1% strain, which marked the onset of loss in adhesion, σ_R was estimated to be close to 20 MPa. The bulk of the loss in adhesion occurred from 2% strain in specimen No. 2, however, for which the radial stress was estimated to be about 60 MPa, taking into account the plastic deformation of the Ti, *i.e.* assuming its Poisson's ratio to be close to 0.5. In specimen No. 1, on the other hand, σ_R was only about 20 MPa under the same conditions. If, on this basis, 20 MPa were to represent a critical radial stress for loss in adhesion one might expect the onset to occur at 2% strain in specimen No. 1. However, as seen from Fig. 2b, loss of adhesion was already apparent at 0.5% strain. The rate of subsequent damage accumulation with increasing strain was significantly less in specimen No. 1 than in specimen No. 2, which might be attributable to the reduced σ_R, but σ_R is clearly not the only factor involved in the damage development. This lower radial stress at the interface for the thinnest coating explains its slower rate of loss of adherence and lower final value shown in Fig. 2b, compared with the thicker coating. However, it is unable to account for the buckling failure, which appeared as patches in the coating bulk and at the interface.

The calculated σ_θ shown in Fig. 10 were compressive and increased linearly with strain in the range considered. The σ_θ for specimen No. 1 were 6% higher in absolute values compared to specimen No. 2, which may contribute to the observed differences in damage morphology (Fig. 6). In fact, there was considerably greater compressive buckling and resulting localized spallation of the coating in case of specimen No. 1, compared to specimen No. 2, in which the dominant interfacial failure mode was delamination. It is the combination of low σ_R and high σ_θ in specimen No. 1 that is thought to be responsible for the compression induced buckling damage in the bulk of the thinnest coating. This is also a further indication of the relatively low cohesive strength of the porous TiO_2 inferred from the Weibull analysis described in the preceding section. The resulting relaxation of σ_R in the fragments explains the maintained adhesion of a residual coating layer to the Ti wire, contrary to specimen No. 1, where interfacial failure apparently precedes compression induced cohesive failure of the coating.

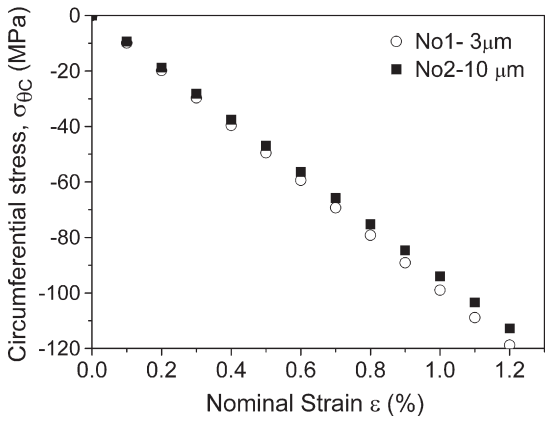

Fig. 10. FEA simulation of the circumferential stress at the interface.

5. Conclusions

The stress state and deformation-induced damage in a TiO_2 coated Ti wire has been analyzed by tensile fragmentation tests and FEA simulations. The experimental investigations and the results of the simulations enabled the adhesion and cohesive strength of the porous TiO_2 coating to be determined. The observations revealed two different damage processes depending on the coating thickness. In case of a 3 μm thick coating, cracks appeared with a broad size distribution and loss of adhesion occurred in patches, with failure taking place both at the interface and within the coating. This implies that a significant proportion of the coating remained attached to the Ti wire at large deformations. In case of a 10 μm thick coating, circumferential cracks appeared at very low strains (0.5%) and their density and width increased with increasing strain. Loss in adhesion was apparent from about 1% strain and propagated rapidly as the strain increased further. The loss of adhesion in this case took place mainly at the interface between the TiO_2 and the Ti. Owing to the relatively high tensile radial stress, just few anchored point persisted. A compromise might be found between PV performance and mechanical integrity (*i.e.*, maintained interface contact during deformation) through thickness optimization, or by reducing Poisson's ratio difference of such systems.

Acknowledgments

The authors would like to thank Konarka Technologies and the Swiss Commission for Technology and Innovation (Project Nr 7228.1 NMPP-NM) for financial support and the Centre Interfacultés de Microscopie Electronique (CIME) of the Ecole Polytechnique Fédérale de Lausanne (EPFL) for technical assistance during the SEM observations.

References

[1] M. Grätzel, Prog. Photovolt. Res. Appl. 8 (2000) 171.
[2] Y. Masuda, W.S. Seo, K. Koumoto, Solid State Ionics 172 (2004) 283.
[3] M. Okuya, K. Nakade, S. Kaneko, Sol. Energy Mater. Sol. Cells 70 (2002) 425.
[4] M.D. Blesic, Z.V. Saponjic, J.M. Nedeljkovic, D.P. Uskokovic, Mater. Lett. 54 (2002) 298.
[5] K. Chittibabu, R. Eckert, R. Gaudiana, L. Li, A. Montello, E. Montello, P. Wormser, U. S. Patent No. US2005/0040374, 24 Feb. 2005.
[6] J. Ramier, C.J.G. Plummer, Y. Leterrier, J.-A.E. Månson, B. Eckert, R. Gaudiana, in Renewable Energy (in press) doi: 10.1016/j.renene.2007.05.029.
[7] J.A. Hautaniemi, J.T. Juhanoja, Surf. Interface Anal. 20 (1993) 421.
[8] M. George, C. Coupeau, J. Colin, J. Grilhe, Thin Solid Films 429 (2003) 267.
[9] M. Verdenelli, S. Parole, F. Chassagneux, J.M. Letoffe, H. Vincent, J.P. Scharff, J. Bouix, J. Eur. Ceram. Soc. 23 (2003) 1207.
[10] C. Xie, W. Tong, Acta Mater. 53 (2005) 477.
[11] D. Müler, E. Fromm, Thin Solid Films 270 (1995) 411.
[12] M.S. Hu, A.G. Evans, Acta Metall. 37 (1989) 917.

[13] Q.D. Yang, M.D. Thouless, S.M. Ward, J. Mech. Phys. Solids 47 (1999) 1337.
[14] F.S. Shieu, M.H. Shiao, Thin Solid Films 306 (1997) 124.
[15] C. Kaya, F. Kaya, B. Su, B. Thomas, A.R. Boccacini, Surf. Coat. Technol. 191 (2005) 303.
[16] D.C. Agrawal, R. Raj, Acta Metall. 37 (1989) 1265.
[17] Y. Leterrier, Prog. Mater. Sci. 48 (2003) 1.
[18] J.W. Hutchinson, Z. Suo, Adv. Appl. Mech. 29 (1992) 63.
[19] S.S. Chakravarthy, E.H. Jordan, W.K.S. Chiu, Eng. Fract. Mech. 72 (2005) 1286.
[20] Y. Leterrier, J. Andersons, Y. Pitton, J.-A.E. Månson, J. Polym. Sci., Part B, Polym. Phys. 35 (1997) 1449.
[21] Y. Leterrier, J. Andersons, Y. Pitton, J.-A.E. Månson, J. Polym. Sci., Part B, Polym. Phys. 35 (1997) 1463.
[22] G. Rochat, Y. Leterrier, P. Fayet, J.-A.E. Månson, Thin Solid Films 437 (2003) 204.
[23] Y. Saito, S. Kambe, T. Kitamura, Y. Wada, S. Yanagida, Sol. Energy Mater. Sol. Cells 83 (2004) 1.
[24] W. Weibull, J. Appl. Mech. 18 (1951) 293.
[25] Y. Leterrier, Y. Wyser, J.-A.E. Månson, J. Adhes. Sci. Technol. 15 (2001) 215.
[26] S.O. Chwa, D. Kleina, F.L. Tomaa, G. Bertranda, H. Liaoa, C. Coddeta, A. Ohmorib, Surf. Coat. Technol. 194 (2005) 215.
[27] M.H. Shiao, F.S. Shieu, Thin Solid Films 358 (2000) 159.